TRANSPIRATION COOLING AT MACH 5 EMPLOYING POROUS UHTC

Hassan Saad Ifti, Tobias Hermann, and Matthew McGilvray

Oxford Thermofluids Institute, Department of Engineering Science, University of Oxford, OX2 0ES, United Kingdom

ABSTRACT

The film effectiveness downstream of a porous UHTC injector on a flat-plate is spatially resolved. The experimental data were obtained in Oxford High Density Tunnel at Mach 5. A flat-plate model was coated with Pressure-Sensitive-Paint to obtain film effectiveness based on coolant concentration. Helium was chosen as the coolant gas, and the blowing ratio and Reynolds number were varied from $F = 0.046\%$ to $F = 0.143\%$ and $Re_u = 8.6{\times}10^6$ m^{-1} to $Re_u = 12.3{\times}10^6$ m^{-1}, respectively. Film effectiveness of up to approximately 40% is found for a blowing ratio of 0.143%. Increasing the blowing ratio by a factor of two is approximately 22.1% more effective at lower Reynolds numbers close to the injector. However, the film diminishes at an approximate stream-wise location of 300 mm, regardless of the blowing ratio. The additional coolant mass flux has no effect further downstream of the injector. Higher blowing ratios result in a higher mixing rate of the film with the cross-flow. The non-uniformity of the porous injector's outflow has a significant, proportional effect on the downstream film, forming a three-dimensional film. It is found that this three-dimensionality is remarkably reduced downstream as the film mixes with the cross-flow at a higher rate downstream of local high mass flux regions.

Index Terms— Transpiration Cooling, Hypersonics, Film Effectiveness, Ultra High Temperature Ceramics (UHTC), Pressure Sensitive Paint (PSP), Thermal Protection System (TPS)

1. INTRODUCTION

Transpiration cooling is a promising technology that could enable a reusable Thermal Protection System (TPS) for hypersonic vehicles such as single-stage rockets or spaceplanes. It is an active cooling method where a coolant gas is injected through a porous material into the boundary-layer. The cooling process is comprised of three different effects: (a) heat from the wall is convected out by the fluid; (b) the coolant gas creates a film that insulates the wall underneath from the hot cross-flow; and (c) the coolant film protects the wall from free-stream Oxygen and thereby prevents oxidation of the wall, which enables the wall-material to operate at a higher temperature enhancing radiative cooling [1, 2]. The success of the latter two processes depends on the coolant film that is formed downstream. This protective film diminishes at a downstream location as it mixes with the incoming hypersonic cross-flow (see Fig. 1), and therefore it is essential to fully understand this mixing process.

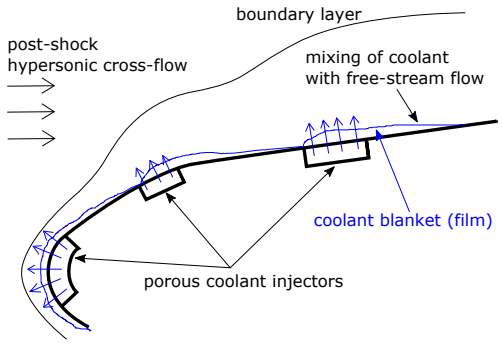

Fig. 1. Schematic of a leading edge of a hypersonic vehicle with porous, transpiration cooling injectors. Note: the blue layers indicate the coolant blankets (not to scale). [1]

In this paper, the mixing process between the transpiring gas and the cross-flow is investigated. A flat-plate model is tested in the Oxford High Density Tunnel (HDT) at Mach 5. A notable amount of work has been done investigating transpiration cooling on flat-plates [3, 4], and therefore a flat-plate geometry is chosen here to continue on that foundation. A flat-plate model also allows to investigate the different phenomena without any geometric complexity. The flat-plate model is instrumented with a porous panel that enables gas injection into the boundary-layer. The porous panel is made of partially sintered Zirconium Diboride (ZrB_2), an Ultra-High-Temperature-Ceramic (UHTC). With pore diameters below 10 μm (see Fig. 2), the injected gas through a porous UHTC is introduced as a bulk into the boundary-layer as opposed to discrete, strong jets as characterised in Ref. [1]. This is important since it is likely that discrete jets could lead to an earlier tripping of the boundary-layer, compared to a relatively uniform mass injection.

In previous work [5] using a porous UHTC injector, it was shown that transpiration cooling requires approximately two orders of magnitude lower blowing ratios to obtain a simi-

lar film effectiveness compared to that of a slot injector. The film effectiveness was measured with Pressure Sensitive Paint (PSP) approximately 50 mm downstream of the injector using Nitrogen as the coolant gas. It was found that the coolant gas forms a 'V' shaped film downstream of the injector due to the lateral mixing with the cross-flow. To further investigate the downstream film effectiveness, the current flat-plate model is designed with a Pressure Sensitive Paint (PSP) coat fully surrounding the porous injector. This enables the determination of the film effectiveness based on coolant concentration downstream of the injector. Helium is used as the coolant. Within the scope of this work, the blowing ratio and Reynolds number are varied from $F = 0.046\%$ to $F = 0.143\%$ and $Re_u = 8.6 \times 10^6$ to $Re_u = 12.3 \times 10^6$ m^{-1}, respectively.

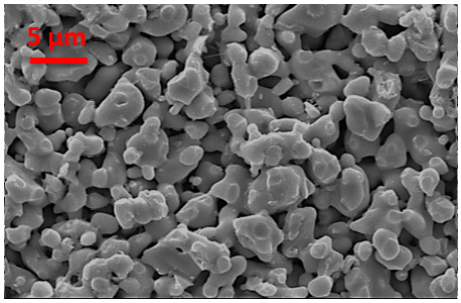

Fig. 2. A ZrB_2 UHTC sample's microstructure (courtesy: Imperial College London).

2. METHODOLOGY

The experiments were conducted in the Oxford High Density Tunnel (HDT) that was operated in its heated Ludwieg tube mode [6] and fitted with a Mach 5 nozzle. Data were acquired on an NI PXIe-8135 controller with NI PXIe-6368 acquisition cards at 2 MS/s/channel. The flat-plate was mounted at an angle of attack of AoA = 0°. The methods of obtaining the required quantities are discussed below.

2.1. Flat-Plate Model

The flat-plate model features a coat of TurboFIB Pressure-Sensitive Paint (PSP) on the surface around the porous injector as shown in Fig. 3. TurboFIB is a single-luminophore, single application PSP that has a response time of under 1 ms. The plate is further instrumented with four flush-mounted Kulite pressure transducers (XCEL-152-25PSIA).

A plenum is attached underneath the porous injector and pipework is in place to feed in the injection gas. The exposed porous area is of 39.5 mm × 39.5 mm. The plenum is fitted with a K-type thermocouple and a Kulite pressure transducer (HEL-375-35BARA) in order to measure the temperature and pressure of the coolant gas, respectively. The reader is referred to Refs. [1, 5] for detailed description of the plenum and injection system.

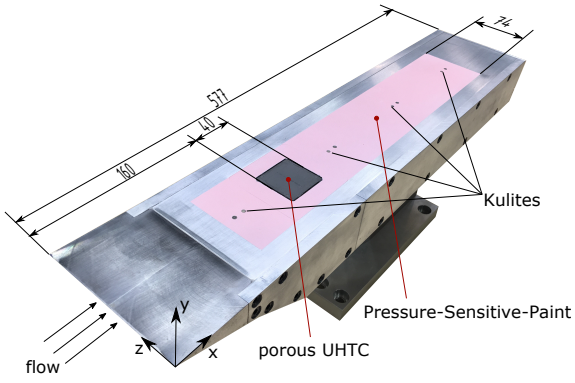

Fig. 3. Flat-plate model with PSP coat.

2.2. Flow Conditions and Blowing Ratios

In the Ludwieg tube mode, pre-heated, pressurised air is released into an evacuated test section by opening a plug valve. The air flows through a plenum and then is accelerated by a Laval nozzle before reaching the test section where the flat-plate model is mounted. The pressure in the plenum upstream of the Laval nozzle is measured and approximated as the total pressure, p_0. The total temperature, T_0, is measured in the test section using differentially heated thin film gauges as described in Ref. [7]. When a shot is fired, the sudden opening of the plug valve releases expansion waves that travel upstream and reflect back downstream. Each of these reflected expansion waves causes a drop in p_0 and T_0, resulting in a change of the flow condition, i.e. the unit Reynolds number, Re_u, as shown in Fig. 4. This feature of the tunnel enables testing at multiple steady conditions – each lasting for approximately 30 ms – from one single shot. The time-averaged unit Reynolds number for steady conditions 1, 2, and 3 (see Fig. 4) are $Re_u = 12.3 \times 10^6$ m^{-1}, $Re_u = 10.3 \times 10^6$ m^{-1}, and $Re_u = 8.6 \times 10^6$ m^{-1}.

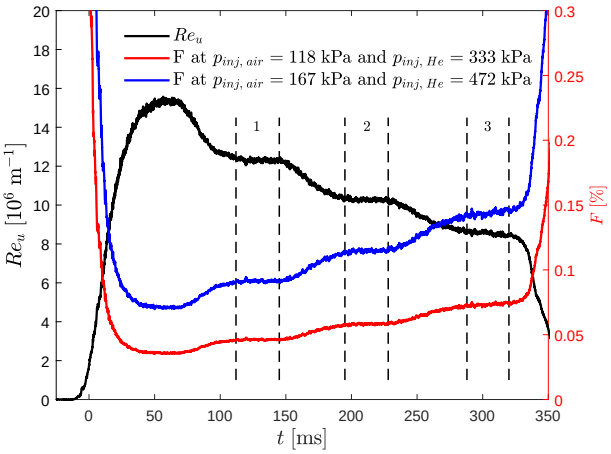

Fig. 4. Unit Reynolds number, Re_u, and blowing ratio, F, versus test time, t, from one single shot.

The static pressure, p_e, is measured by the pressure transducers instrumented on the flat-plate. The edge Mach number, M_e, is obtained from the isentropic flow equations using the ratio of static-to-total pressure, $\frac{p_e}{p_0}$. Subsequently, the edge temperature, T_e, and edge density, ρ_e, are calculated using the isentropic flow equation and the ideal gas law, respectively. The edge velocity is calculated by the equation

$$u_e = M_e\sqrt{\gamma R T_e}, \tag{1}$$

where γ and R are the isentropic exponent and specific gas constant of air. The unit Reynolds number is obtained from the equation

$$Re_u = \frac{\rho_e u_e}{\mu(T_e)}, \tag{2}$$

where $\mu(T_e)$ is the dynamic viscosity of the flow. Since $T_e < 89$ K, Keyes' viscosity model [8], given as

$$\mu(T_e) = \frac{1.488\times10^{-6}\sqrt{T_e}}{1+\frac{122.1}{T_e}\times10^{-\frac{5}{T_e}}}, \tag{3}$$

is employed. The obtained transient unit Reynolds number is plotted in Fig. 4.

The blowing ratio, i.e. the ratio of the injected coolant mass flux to the boundary-layer edge mass flux, is defined as

$$F = \frac{\rho_c u_c}{\rho_e u_e}, \tag{4}$$

where the subscript 'c' denotes coolant quantities at the surface. Due to continuity, the mass flux in the plenum and the mass flux injected into the boundary-layer are equal, hence

$$\rho_c u_c = \rho_{inj} u_{inj}, \tag{5}$$

where the subscript 'inj' stands for quantities inside the plenum. The density of the coolant can be obtained from the ideal gas law,

$$\rho_{inj} = \frac{p_{inj}}{R_c T_{inj}}, \tag{6}$$

where R_c is the specific gas constant of the coolant gas. Substituting Eq.(2), Eq.(4), Eq.(5), Eq.(6), and $p_{out} = p_e$ in the integrated version of the Darcy-Forchheimer equation (see Ref. [1]) yields a form of the Darcy-Forchheimer equation that is directly dependent on the blowing ratio and unit Reynolds number given as follows:

$$\frac{p_{inj}^2 - p_e^2}{2LR_cT_{inj}} = \frac{Re_u\mu(T_e)\mu_c(T_{inj})}{K_D}F + \frac{(Re_u\mu(T_e))^2}{K_F}F^2. \tag{7}$$

The values of permeability coefficients, K_D and K_F, were determined in a dedicated ISO 4022 standard test rig at the Oxford Thermofluids Institute [1]. The obtained values for the sample used in this paper, i.e. UHTC-6, are given in Table 1 with their corresponding uncertainties.

sample ID	K_D [10^{-14} m^2]	K_F [10^{-7} m]	L [mm]
UHTC-6	3.731 ± 0.073	1.538 ± 0.333	5

Table 1. Permeability coefficients and their corresponding uncertainties for UHTC-6 [1].

With a known unit Reynolds number, Re_u, and a plenum pressure, p_{inj}, the positive solution to Eq.(7) with respect to 'F' directly yields the blowing ratio. Note that the gas temperature, T_{inj}, measured by the thermocouple in the plenum is close to room temperature, and therefore the coolant gas viscosity, $\mu_c(T_{inj})$, is calculated using Sutherland's model [9] with appropriate constants for the coolant gas in use. When HDT is fired, a constant gas pressure is set in the plenum by the gas injection system in the HDT. This plenum pressure, p_{inj}, is measured during each test by the pressure transducer fitted in the plenum. In Fig. 4, the transient blowing ratios obtain from Eq.(7) are illustrated for two different plenum pressures. Since the unit Reynolds number drops over time during the whole test period, the blowing ratio increases over time. Similar to the unit Reynolds number, the blowing ratio remains almost constant over a time period of approximately 30 ms for each steady condition.

The outflow distribution of the employed porous injector is characterised by hot-wire anemometry with air injection. Details of the process can be found in Ref. [1]. The obtained velocity map is illustrated in Fig. 5. This particular injector features significant non-uniformities. Local high velocity regions can be observed, especially on the edges. A region of significantly lower permeability is noticeable in the middle of the injector.

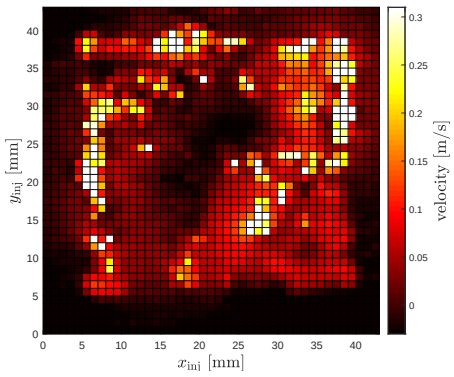

Fig. 5. Velocity map of the porous UHTC injector. Injected gas: air.

2.3. Pressure-Sensitive-Paint (PSP)

A Luminus PT-120-TE UV high power LED is positioned above the model. The LED is turned on for approximately 2 minutes before each shot to allow for repeatable illumination between shots. The emitted radiation passes by a UV bandpass filter with a central wavelength of 390 nm and a

full width at half maximum of 125 nm. A diffusor is placed underneath the LED to improve the even spread of the UV radiation on the PSP surface of the model. The luminophore in the TurboFIB PSP is excited by the UV radiation and achieves a higher state of energy that results in an emission in the red wavelength spectrum as it returns to its ground state. The difference between the absorbed and emitted radiation's wavelength is referred to as the Stokes shift [10]. A larger Stokes shift, as the case here, is desirable for PSPs since it is easier to distinguish the two. The emitted radiation from the PSP reflects off a flat mirror and is captured by a high-speed camera (Photron FASTCAM Mini AX200 type 900K) that is fitted with a red filter and placed outside the test section. The images are captured at a frame rate of 8100 fps, shutter speed of 55.56 μs, a bit depth of 12, and a resolution of 1024×512. The acquisition of images is started before the flow arrival and continued for the whole duration of the test. The images are warped and passed through an image stabilisation algorithm prior to post-processing.

The excitation of PSP luminophores is quenched by oxygen [11], and therefore an increase in Oxygen partial pressure, p_{O_2} results in a lower intensity, I, of the emitted radiation, and vice-versa. This characteristic can be expressed in the power law form of the Stern-Volmer equation as

$$\frac{I_{ref}}{I} = c_1 \left(\frac{p_{O_2}}{p_{O_2,\,ref}} \right)^n + c_2,\ 0 < n \leq 0.5. \qquad (8)$$

Here, I_{ref} and $p_{O_2,\,ref}$ respectively refer to intensity and pressure reference values taken before the flow arrival. The coefficients, c_1, c_2, and n are determined by a regression analysis from calibrated data. For this test campaign, the reference values, I_{ref} and $p_{O_2,\,ref}$, were taken prior to the flow arrival when the test section is approximately in a vacuum (7.7 Pa to 8.4 Pa). All pressure values are time-averaged from the pressures measured by the pressure transducers instrumented in the model and multiplied by 0.21 in order to obtain the partial pressure of Oxygen. The calibration is performed by collecting data from a shot without injecting any coolant gas. The spatially averaged R-squared value for this calibration is $R^2 = 0.994$. Since the same calibration is applied to all the other shots with gas injection, a trace of the film can be identified as the quenching is influenced by the film. Injected Helium gas hinders the quenching by displacing air in the boundary-layer. Comparing a case with air injection and one with a foreign gas injection at the same blowing ratio, in this case Helium, gives a measure of how much air is displaced by the foreign gas, i.e. to what extent the foreign gas is forming a film. This measure is given by the film effectiveness expressed as [12]

$$\eta_c = \frac{C_w - C_e}{C_c - C_e} = 1 - \frac{1}{\left(\frac{p_{O_2,\,\text{air}}}{p_{O_2,\,\text{foreign gas}}} - 1 \right) \frac{W_{\text{foreign gas}}}{W_{\text{air}}} + 1}, \qquad (9)$$

where C is the concentration and subscript 'w' stands for concentration at the wall; $p_{O_2,\,\text{air}}$ and $p_{O_2,\,\text{foreign gas}}$ are Oxygen partial pressures with air and foreign gas injections, respectively, at the same blowing ratio. W_{air} and $W_{\text{foreign gas}}$ denote the respective molar masses. A film effectiveness of $\eta_c = 1$ corresponds to a full displacement of the air by the foreign gas, whereas $\eta_c = 0$ indicates that no displacement of air is achieved and the film is fully diminished. Since η_c is calculated for every pixel, it yields a spatial map of the whole film downstream of the porous injector. Essentially, this film effectiveness based on coolant concentration quantifies the physical presence of the film in terms of its concentration.

In Fig. 6, the Oxygen partial pressure map at $Re_u = 8.6 \times 10^6$ m^{-1} with air injection at $F = 0.143\%$ is presented. This map is obtained by applying the aforementioned calibration. Here, the average Oxygen partial pressure measured by the transducers is $p_{O_2} = 0.24$ kPa. This map shows that there is no noticeable effect of the film itself on the pressure field downstream of the injector. The deviation in pressure at the corners is a result of higher noise stemming from the relatively higher movement of the mirror and an uneven spread of the UV radiation.

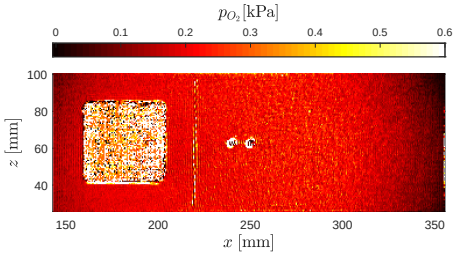

Fig. 6. Spatial map of Oxygen partial pressure at $Re_u = 8.6 \times 10^6$ m^{-1}, $F = 0.143\%$. Injected gas: air.

3. RESULTS

Contour plots of the film effectiveness based on coolant concentration obtained from PSP are presented in Fig. 7. Results for six different blowing ratios, ascending from (a) to (f), are shown for a total of three different unit Reynolds numbers.
In Fig. 7, it can be observed that the film effectiveness, η_c, increases overall as the blowing ratio, F, is increased. For all blowing ratios, the film effectiveness is higher right after the porous injector and reduces in the stream-wise direction as the film mixes with the cross-flow and diminishes downstream. For the highest blowing ratio, $F = 0.143\%$, the maximum effectiveness is approximately 0.4, i.e. 40% of the injected Helium is present at the wall. In all cases, the film does not exhibit the 'V' shape as shown in Ref. [5]. In addition, it can be observed in Fig. 7 that the film is stronger on the edges in all cases, displaying a fully three-dimensional behaviour. It can be further noticed that the bottom edge (at approximately $z = 50$ mm) of the film has a higher effectiveness compared to the upper edge. This three-dimensional

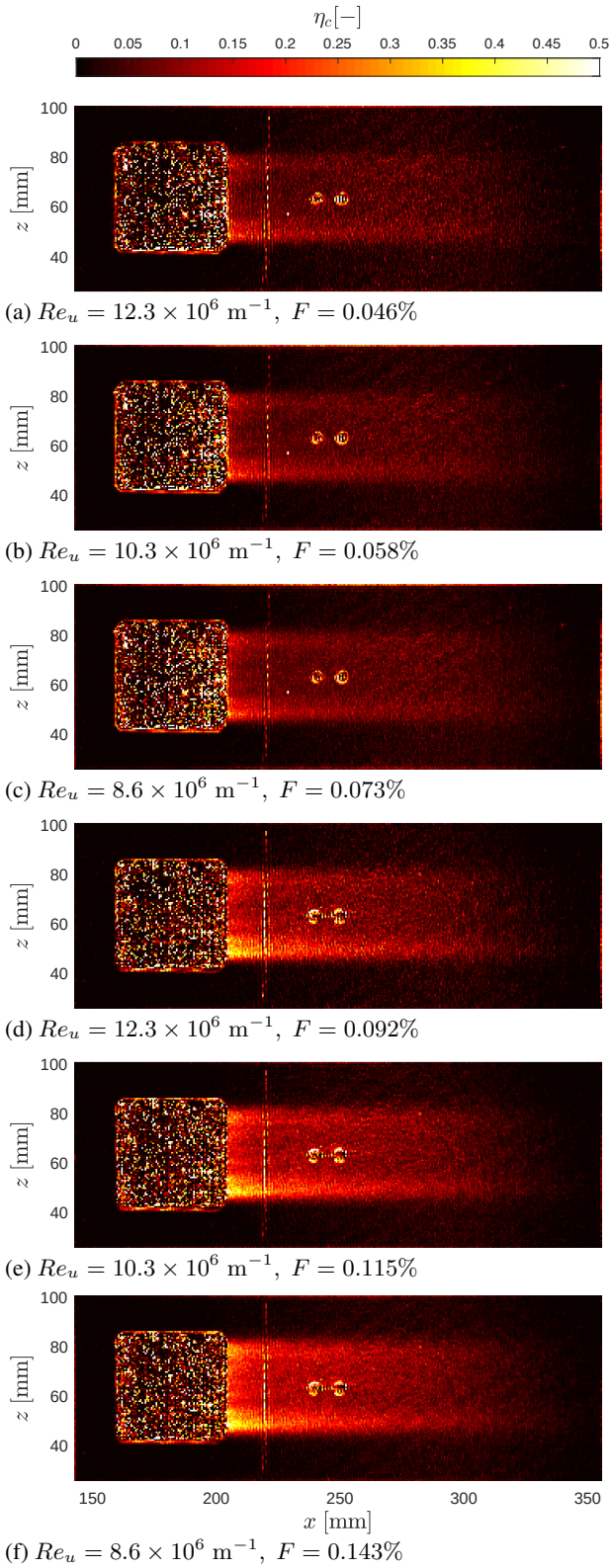

(a) $Re_u = 12.3 \times 10^6$ m^{-1}, $F = 0.046\%$

(b) $Re_u = 10.3 \times 10^6$ m^{-1}, $F = 0.058\%$

(c) $Re_u = 8.6 \times 10^6$ m^{-1}, $F = 0.073\%$

(d) $Re_u = 12.3 \times 10^6$ m^{-1}, $F = 0.092\%$

(e) $Re_u = 10.3 \times 10^6$ m^{-1}, $F = 0.115\%$

(f) $Re_u = 8.6 \times 10^6$ m^{-1}, $F = 0.143\%$

Fig. 7. Contours of downstream film effectiveness, η_c, obtained from PSP data.

behaviour is consistent with the outflow characteristic illustrated in Fig. 5, where the permeability of the injector is low in the middle. This infers that the uniformity of the injector's outflow has a significant effect on the film downstream.

Span-wise averaged values of effectiveness, η_c, over the whole film area are plotted in Fig. 8. For each unit Reynolds number, i.e. (a) to (c), there is a significant rise in effectiveness when the blowing ratio is doubled. This trend becomes more prominent as the unit Reynolds number decreases from (a) to (c). Hence, increasing the blowing ratio in lower Reynolds numbers is more effective, suggesting that the inertial force of the cross-flow is a major factor in the mixing process. It can be further noticed that regardless of the blowing ratio, η_c collapses after approximately $x = 300$ mm and diminishes completely. This shows that although a higher blowing ratio can result in a higher effectiveness close to the injector, it does not necessarily retain it further downstream. The high momentum from a higher blowing ratio eventually promotes the mixing. There is no effect of additional coolant mass injection further downstream of the injector. Furthermore, it can be observed that the rate of mixing or decay of the film is significantly higher when the blowing ratio is doubled. Doubling the blowing ratio leads to a rise in effectiveness almost by a factor of two close to the injector, but this rise decreases in the stream-wise direction and becomes non-existent further downstream. For each Reynolds number, the lower blowing ratio results in a plateaued film between approximately $x = 220$ mm to $x = 280$ mm, whereas the steeply falling slope is apparent when the blowing ratio is doubled. This suggests that a constant coverage of the film downstream is achievable with lower blowing ratios, i.e. lower coolant mass flux.

Since the film exhibits a three-dimensional behaviour, the lateral spread of it is also of interest. In Fig. 9, stream-wise averaged values of effectivenesses, η_c, over $x = 217$ mm to $x = 240$ mm are illustrated. For all cases, (a) to (c), the asymmetrical shape of the film is clearly visible. The aforementioned bias towards the left, at approximately $z = 50$ mm, is also noticeable. Moreover, the effect of doubling the blowing ratio is clearly noticeable, which becomes more prominent with dropping Reynolds numbers and rising blowing ratios, (a) to (c), as observed in the results shown for the span-wise averaged values in Fig. 8 (up to 22.1%).

In order to visualise the three-dimensional behaviour of the film as it convects downstream, stream-wise averaged film effectivenesses over $x = 205$ mm to $x = 215$ mm (black), $x = 253$ mm to $x = 266$ mm (green), and $x = 278$ mm to $x = 290$ mm (red) are plotted in Fig. 10. For each Reynolds number and blowing ratio, (a) to (c), it is noticeable that the three-dimensional behaviour reduces as the film convects downstream. The non-uniformity seen close to the injector (black curve) is significantly flattened further downstream (green and red curves). Depending on the non-uniformity of the film, the effectiveness is divided in three different regions:

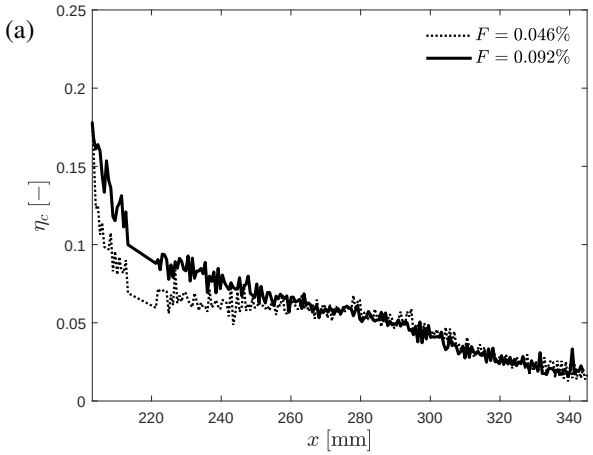

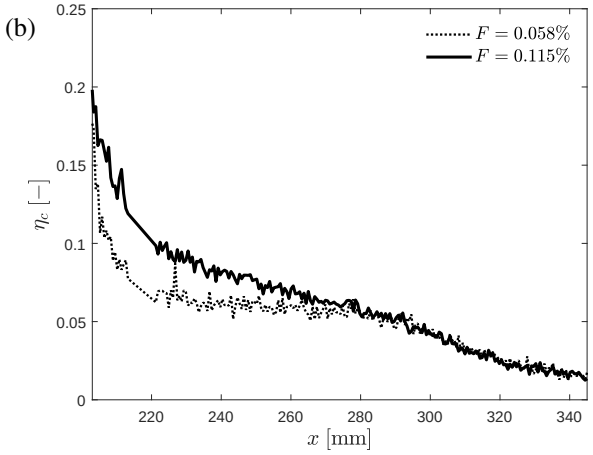

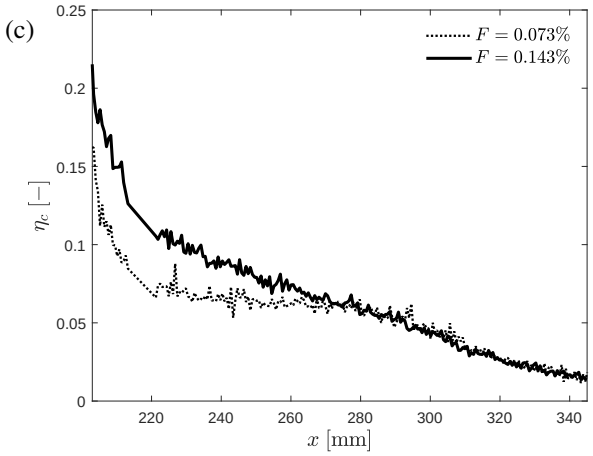

Fig. 8. Span-wise averaged film effectiveness, η_c, versus distance in the stream-wise direction, x, at (a) $Re_u = 12.3 \times 10^6$ m^{-1}, (b) $Re_u = 10.3 \times 10^6$ m^{-1}, and (c) $Re_u = 8.6 \times 10^6$ m^{-1}.

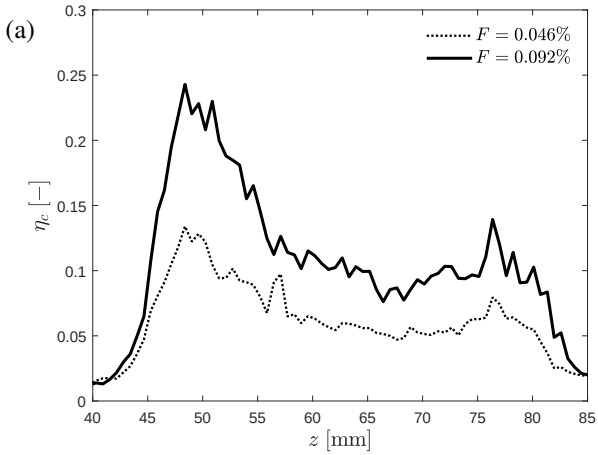

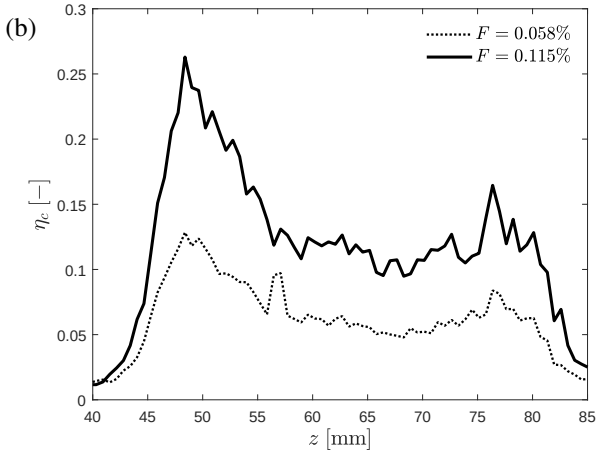

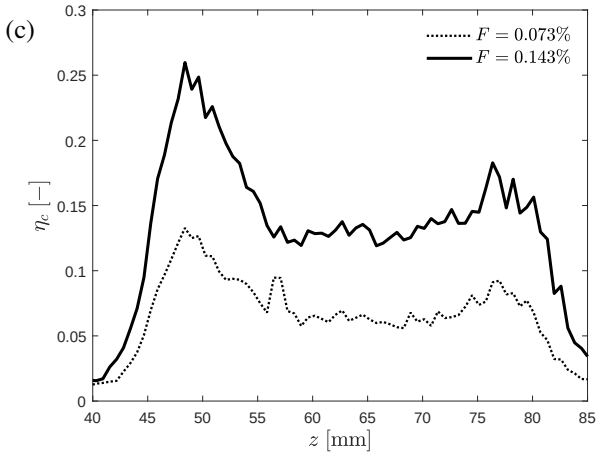

Fig. 9. Stream-wise averaged ($x = 217$ mm to $x = 240$ mm) film effectiveness, η_c, versus distance in the span-wise direction, z, at (a) $Re_u = 12.3 \times 10^6$ m^{-1}, (b) $Re_u = 10.3 \times 10^6$ m^{-1}, and (c) $Re_u = 8.6 \times 10^6$ m^{-1}.

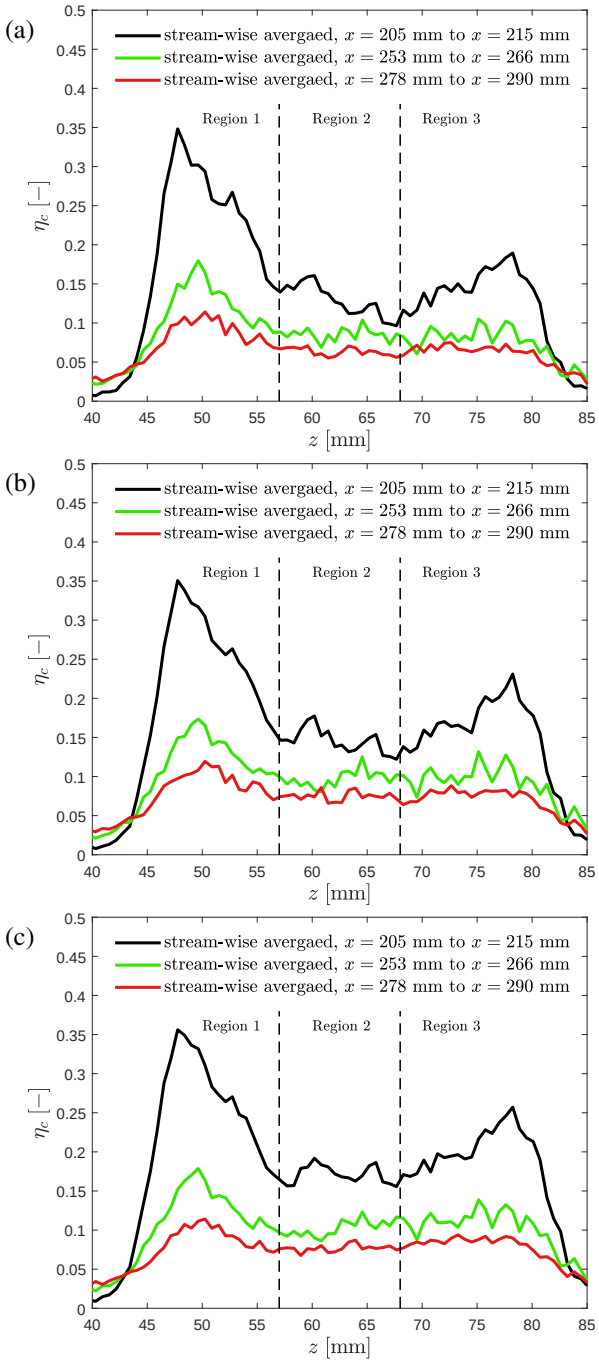

Fig. 10. Stream-wise averaged (over three different stream-wise locations) film effectiveness, η_c, versus distance in the span-wise direction, z, at (a) $Re_u = 12.3 \times 10^6$ m^{-1}, $F = 0.092\%$, (b) $Re_u = 10.3 \times 10^6$ m^{-1}, $F = 0.115\%$, and (c) $Re_u = 8.6 \times 10^6$ m^{-1}, $F = 0.143\%$.

Region 1, Region 2, and Region 3 as annotated in Fig. 10. Here, Region 1 has the highest effectiveness and Region 2 the lowest. This is consistent with outflow velocity distribution of the injector (see Fig. 5). For reference, the approximate average mass fluxes at Region 1, Region 2, and Region 3 on the injector are respectively 39%, 27%, and 34% of the total injected mass flux. These values are obtained from a bench-top test with air injection at 2 bar. For each Reynolds number, (a) to (c), the rate of drop in effectiveness is the highest in Region 1 and the lowest in Region 2, suggesting that the higher mass flux, and hence higher momentum flux, results in a stronger mixing between the coolant and the cross-flow. This effect is further demonstrated in Fig. 11, where the span-wise averaged effectiveness is plotted for Region 1, Region 2, and Region 3 at $Re_u = 8.6 \times 10^6$ m^{-1}, $F = 0.143\%$. It can be seen that the discrepancy in the effectiveness amongst the three regions is significantly higher close to the injector. This discrepancy reduces as the film convects downstream and eventually becomes close to zero as the three-dimensionality disappears. From $x = 225$ mm to $x = 320$ mm, the rates of decay for Region 1, Region 2, and Region 3 are respectively $\frac{\partial \eta_c}{\partial x} = 0.0018$ mm^{-1}, $\frac{\partial \eta_c}{\partial x} = 0.0011$ mm^{-1}, and $\frac{\partial \eta_c}{\partial x} = 0.0014$ mm^{-1}, confirming that the film in regions with higher momentum flux have higher decay rates. This reiterates that a lower blowing ratio, i.e. coolant mass flux, could be enough to form a relatively constant film downstream.

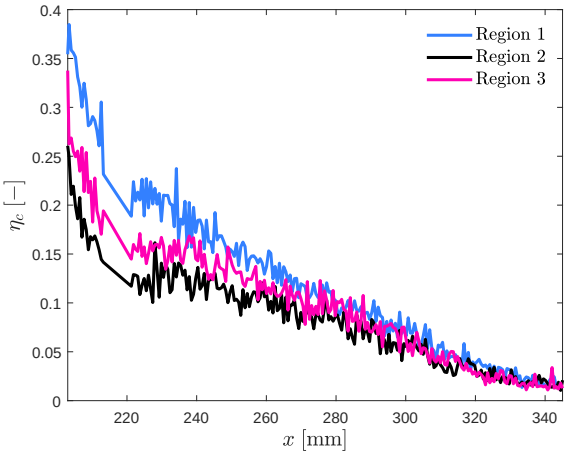

Fig. 11. Span-wise averaged film effectiveness, η_c, over Region 1, Region 2, and Region 3 versus distance in the stream-wise direction, x, at $Re_u = 8.6 \times 10^6$ m^{-1}, $F = 0.143\%$.

4. CONCLUSION

A transpiration cooled flat-plate instrumented with a porous Ultra-High-Temperature-Ceramic (UHTC) is tested in the Oxford High Density Tunnel (HDT) at Mach 5. The flat-plate model features a coat of TurboFIB Pressure-Sensitive-Paint that is used to determine the downstream film effectiveness based on coolant concentration. Helium is injected as the coolant gas. Data are presented for three different unit Reynolds numbers, i.e. $Re_u = 8.6 \times 10^6$ m^{-1}, $Re_u = 10.3 \times 10^6$ m^{-1}, and $Re_u = 12.3 \times 10^6$ m^{-1}, and six

blowing ratios ranging from $F = 0.046\%$ to $F = 0.143\%$. For all blowing ratios, the film is stronger as it exits the porous injector and becomes weaker in the stream-wise direction as it convects downstream and eventually diminishes due to its mixing with the cross-flow. For the highest blowing ratio, $F = 0.143\%$, the maximum effectiveness is approximately 0.4. Doubling the blowing ratio is more effective at lower unit Reynolds numbers close to the injector; however, the film starts diminishing at an approximate stream-wise location of 300 mm, regardless of the blowing ratio and Reynolds number. The additional coolant mass injection has no effect on the effectiveness further downstream of the injector. The film mixes at a higher rate when the blowing ratio, i.e. coolant mass flux is increased. The non-uniformity of the porous injector's outflow has a significant effect on the downstream film effectiveness, which results in a three-dimensional film. Local high mass flux values in the outflow result in higher film effectiveness downstream of the corresponding locations. This three-dimensionality, however, reduces as the film convects downstream. This is due to the fact that the mixing or decay rate of the downstream film effectiveness of high mass flux areas is higher. Therefore, the discrepancy in effectiveness in the span-wise direction reduces as the film convects downstream. For future work, it is foreseen to conduct experiments in a wider range of Reynolds numbers and blowing ratios. Moreover, testing different porous injectors, including varying permeability, is seen as an important way forward since the non-uniformity of the outflow of the injector has a significant effect on the downstream film effectiveness. It is further planned to spatially resolve the thermal film effectiveness employing Infrared Thermography.

Acknowledgements

The funding for this research by the EPSRC grant 'Transpiration Cooling Systems for Jet Engine Turbines and Hypersonic Flight' (reference: EP/P000878/1) is duly acknowledged. The authors of this paper would like to thank the following people: Chris Hambidge, Dr Peter Forsyth, Dr Laurent Le Page, and Imran Naved for their active assistance during this test campaign; Gregory King for his support during the instrumentation phase; Brian Eade and Duncan Constable for machining the model-parts.

References

[1] Hassan Saad Ifti, Tobias Hermann, and Matthew McGilvray, "Flow Characterisation of Transpiring Porous Media for Hypersonic Vehicles," in *22nd AIAA International Space Planes and Hypersonics Systems and Technologies Conference*, Reston, Virginia, Sept. 2018, p. 412, American Institute of Aeronautics and Astronautics.

[2] Marc Ewenz Rocher, Matthew McGilvray, Tobias A Hermann, Hassan S Ifti, Fabian Hufgard, Martin F Eberhart, Arne Meindl, Stefan Loehle, Tommaso Giovannini, and Luc J Vandeperre, "Testing a Transpiration Cooled Zirconium-Di-Boride sample in the Plasma Tunnel at IRS," in *AIAA Scitech 2019 Forum*, Reston, Virginia, Jan. 2019, p. 01, American Institute of Aeronautics and Astronautics.

[3] A Gülhan and S Braun, "An experimental study on the efficiency of transpiration cooling in laminar and turbulent hypersonic flows," *Experiments in Fluids*, vol. 50, no. 3, pp. 509–525, Aug. 2010.

[4] H Tanno, T Komuro, K Itoh, Markus Kuhn, Ivaylo Petkov, and B Esser, "Transpiration cooling experiments in free-piston shock tunnel HIEST," July 2016.

[5] T Hermann, H S Ifti, M McGilvray, L Doherty, and R P Geraets, "Mixing characteristics in a hypersonic flow around a transpiration cooled flat plate model," 2018.

[6] Matthew McGilvray, Luke J Doherty, Andrew J Neely, Robert Pearce, and Peter Ireland, "The Oxford High Density Tunnel," in *20th AIAA International Space Planes and Hypersonic Systems and Technologies Conference*, Reston, Virginia, July 2015, p. 17, American Institute of Aeronautics and Astronautics.

[7] Tobias Hermann, Matthew McGilvray, Chris Hambidge, Luke Doherty, and David Buttsworth, "Total Temperature Measurements in the Oxford High Density Tunnel," in *International Conference on Flight vehicles, Aerothermodynamics and Re-entry Missions and Engineering, FAR*, Monopoli, Italy, 2019.

[8] Frederick G Keyes, "The Heat Conductivity, Viscosity, Specific Heat and Prandtl Numbers for Thirteen Gases.," Apr. 1952.

[9] William Sutherland, "LII. The viscosity of gases and molecular force," *The London, Edinburgh, and Dublin Philosophical Magazine and Journal of Science*, vol. 36, no. 223, pp. 507–531, 1853.

[10] Joseph R Lakowicz, *Principles of Fluorescence Spectroscopy*, Springer US, Boston, MA, 2006.

[11] Mark Kenneth Quinn, Leichao Yang, and Konstantinos Kontis, "Pressure-Sensitive Paint: Effect of Substrate," *Sensors*, vol. 11, no. 12, pp. 11649–11663, Dec. 2011.

[12] Muhammad Hassan Bashir, Chao-Cheng Shiau, and Je-Chin Han, "Film cooling effectiveness for three-row compound angle hole design on flat plate using PSP technique," *International Journal of Heat and Mass Transfer*, vol. 115, pp. 918–929, Dec. 2017.